Environmental Science Advances

PAPER

View Article Online
View Journal | View Issue

Cite this: *Environ. Sci.: Adv.*, 2023, **2**, 247

Catalytic degradation of methylene blue dye and antibacterial activity of biosynthesized silver nanoparticles using *Peltophorum pterocarpum* (DC.) leaves

Segun Ajibola Ogundare,[ab] Titilayo Oyeronke Adesetan,[c] Gregarious Muungani,[a] Vashen Moodley,[a] James Friday Amaku,[d] Odunayo Christy Atewolara-Odule,[b] Sodiq Tolulope Yussuf,[b] Nurudeen Olanrewaju Sanyaolu,[b] Adeola Ahmed Ibikunle,[b] M.-Sadeeq Balogun[e] and Werner Ewald van Zyl*[a]

We report the use of the aqueous extract of *Peltophorum pterocarpum* leaves (PPLE) as a source of relatively cheap and readily accessible reducing- and stabilizing agents for the biosynthesis of silver nanoparticles (AgNPs). The biosynthesis was conducted at 80 °C and pH 9 within 45 min. The FTIR and UV-vis spectroscopic characterization of the PPLE provided evidence of chromophores with functional groups characteristic of polyphenolic compounds. These associated functional groups were also observed in the FTIR spectrum of the AgNPs which suggested their influence on the stabilization of the AgNPs. Similarly, the SEM micrograph and TGA thermogram indicated the presence of PPLE phytoconstituents on the surface of the synthesized AgNPs. The crystalline nature of the AgNPs was noted by the rings in the SAED obtained from HRTEM, which also showed the AgNPs as spheres and ellipses with sizes in the range of 2–50 nm. The AgNPs showed good catalytic activity in the degradation of methylene blue dye with a pseudo-first-order rate constant of 0.3378 min^{-1}. The degradation was completed within 6 min. In addition, the AgNPs displayed improved antibacterial activities in comparison with the PPLE against selected clinical pathogens. Based on our findings in this study, the AgNPs can serve as a potential catalyst in water treatment and also as an antimicrobial agent in disinfectant formulations.

Received 20th July 2022
Accepted 24th November 2022

DOI: 10.1039/d2va00164k

rsc.li/esadvances

Environmental significance

Industrialization has brought great economic development, but it is associated with enormous environmental challenges that include the pollution of water bodies with effluents containing toxic and non-biodegradable chemicals. Methylene blue (MB) dye is a common coloring agent in the paper and textile industries. At a high level in industrial effluents, it can impact both human and aquatic life negatively. Hence, there is an essential need to reduce it to a less harmful form by chemical degradation, which requires the use of a suitable catalyst. The catalyst should be generated in an environmentally friendly and sustainable manner. We demonstrate the use of *Peltophorum pterocarpum* leaf extract (PPLE) as a source of polyphenolic compounds suitable as reducing and stabilizing agents in the biosynthesis of silver nanoparticles (AgNPs). The catalytic and antimicrobial activities of the biosynthesized AgNPs make them suitable for the chemical degradation of MB dye and as an antimicrobial agent for disinfectant formulation.

1. Introduction

Peltophorum pterocarpum (PP), commonly referred to as copper pod, is a plant well known in many parts of the world as an ornamental tree. Its golden yellow flower and dark brownish pod as well as widespread canopy along the coastal and inland areas provide shelter from the sun.[1] Similarly, its ubiquitous nature makes it accessible for the exploration of its extracts in traditional medicine for the treatment of diverse ailments and also as a source of dye used in the tanning of leather.[2] The leaf, flower, pod and stem bark extracts of PP have been claimed to provide relief from toothaches, intestinal disorders, muscular

[a]*School of Chemistry and Physics, University of KwaZulu-Natal, Westville Campus, Durban, 4000, South Africa. E-mail: vanzylw@ukzn.ac.za*
[b]*Department of Chemical Sciences, Olabisi Onabanjo University, P. M. B. 2002, Ago-Iwoye, Nigeria*
[c]*Department of Microbiology, Olabisi Onabanjo University, P. M. B. 2002, Ago-Iwoye, Nigeria*
[d]*Department of Chemistry, Michael Okpara University of Agriculture, Umudike, Nigeria*
[e]*College of Materials Science and Engineering, Hunan University, Changsha, 410082, Hunan, China*

pain, eye irritation, and skin infection, and they are known to aid rapid healing of sores.[2–4] These claims have become the subject of recent scientific investigations with findings leading to the establishment of the antioxidant, antidiabetic, anticancer, antimicrobial, anticoagulant, cytotoxic, estrogenic, antiglycaemic, hepatoprotective, urolithiasis, aldose reductase, and acetyl choline esterase inhibitory activities of PP,[3–11] which are associated with the presence of phytochemicals that include flavonoids, terpenoids, polyphenols, steroids, tannins, glycosides, and alkaloids.[1,3,5–7,9,11,12]

The versatility of the leaf extract (LE) of PP has been explored as a source of natural dyes in the fabrication of dye-sensitized solar cells. This is attributed to the presence of anthocyanin and carotene.[13–16] Other chemical constituents of PPLE have also been identified as phenoxychromones, naringenins, ophioglonins, kaempferol, luteolin, isohamnetin, chrysoeriol, quercetins, and pachypodol,[11,17–19] which are generally polyphenols with strong antioxidant activities hence they account for the health benefits associated with the use of PPLE.[20] The chemical constituents of PPLE make it a potential source of reducing and stabilizing agents for the green synthesis of nanoparticles (NPs).[21,22] NPs are currently included in many commercial products and as such, the use of nature-based reducing and stabilizing agents is essential in their production to ensure a reduction in toxicity and environmental hazard associated with the use of conventional synthetic chemicals in the production.[23–25] Among the numerous NPs added to commercial products, silver (Ag) NPs are the most prominent as they are added to home appliances, food packaging, electronics, computers, textiles, personal care products, children's toys, and kitchen wares, and as food supplements under different trade names.[26–29] This is mostly to impart antimicrobial activities to the products. The inclusion of AgNPs has been found to increase the shelf-life of perishable food items and enhance the healing of wounds as well as minimize bacterial growth in many appliances.[26] Although there are concerns about the impact of AgNPs in commercial products and the consequences of their accumulation in the environment, there have been no established cases of AgNP toxicity or negative influence on the environment. Generally, research findings revealed that the benefit of AgNP usage outweighed the yet-to-be-established consequences.[26] Indeed, this does not call for liberal or indiscriminate use of AgNPs rather it requires the adoption of a green method for production to ensure biodegradability and prevent bioaccumulation. The green approach is sustainable, and simple and does not lead to the generation of hazardous waste associated with the classical colloidal chemistry approaches.

AgNPs have shown tremendous benefits, which also include their potential ability to reduce the accumulation of non-biodegradable organic pollutants found in the effluents of many manufacturing industries.[30] Methylene blue (MB) dye is one of the organic pollutants present in the effluents of industrial facilities making use of it as a pigment and colorant. Its accumulation and persistence in water bodies negatively impact aquatic life. Hence, the regular need for its reduction to safety limits is a priority in the treatment of industrial effluents. One of the methods considered suitable is chemical degradation using sodium borohydride ($NaBH_4$). The process required the use of a catalyst to reduce the duration of the reaction to meet the rate of effluent discharge from the manufacturing plants. AgNPs are a suitable catalyst for increasing the rate of reaction. In recent times, there have been reports on the catalytic degradation of MB dye using metal NPs synthesized by green methods;[30–32] however, the catalytic activities of the nanoparticles vary with respect to the shape and dimension of the NPs, and the search is still ongoing for catalysts with improved performance. In this study, we investigated the use of PPLE in the eco-friendly green synthesis of AgNPs and consider their potential as a catalyst in the chemical reduction of MB dye and also their antimicrobial activity against clinical pathogens with a perspective to produce AgNPs that can be included in commercial products and as well suitable as a catalyst in the degradation of MB dye. Our chosen PPLE is based on its known benefits and its ubiquitous nature. This will make it readily accessible for the eco-friendly synthesis of AgNPs on large scale.

2. Experimental details

2.1. Materials

Fresh leaves of PP were obtained from Olabisi Onabanjo University, Ago-Iwoye Campus, Ogun State, Nigeria. Sodium hydroxide pellets (NaOH), nitric acid (HNO_3, 69% w/w), silver nitrate ($AgNO_3$), sodium borohydride ($NaBH_4$) and methylene blue dye reagent grade were procured from Sigma-Aldrich and used as received. Distilled water was used in all preparations.

2.2. Preparation of PPLE

Freshly obtained PP leaves were washed twice to remove extraneous substances (mainly dust). The aqueous extraction of the leaves was done by adding 10 g of the dry leaves to 200 mL of water; equivalent to 50 g L^{-1}. The aqueous mixture was maintained at 90 °C for 45 min using a magnetic stirrer. This was followed by cooling to room temperature and filtering using Whatman No. 1 filter paper to obtain the PPLE which was used for the preparation of AgNPs. The volume of the extract was adjusted appropriately to maintain the concentration. The dry sample of PPLE was obtained by heating the solution in an oven maintained at 50 °C for 2 h.

2.3. Biosynthesis of AgNPs using PPLE

The eco-friendly green synthesis of AgNPs was preceded by a preliminary procedure to establish suitable conditions for the synthesis. This involved varying the volume of PPLE, pH, temperature, and time. The optimized synthesis was finally conducted at 80 °C using the PPLE (200 mL) and 1 mM $AgNO_3$ (40 mL) in a volume ratio of 20/4 with the pH adjusted to 9 using 0.1 M NaOH. The reaction was maintained at 80 °C for 45 min. The obtained dark brown product was recovered by centrifugation at 10, 000 rpm for 30 min and washed with distilled water. This procedure was repeated to eliminate unreacted metal precursors. The volume of the obtained product was adjusted to 200 mL and then sonicated to obtain a homogenous dispersion. The percentage of Ag in the solution was

determined by Inductive Coupled Plasma Optical Emission Spectroscopy (ICP-OES) after microwave digestion in nitric acid (69% w/w). A dry sample of the biosynthesized AgNPs used for characterization was obtained by drying in an oven at 50 °C 2 h.

2.4. Characterization

The reduction of Ag ions to AgNPs was observed by UV-vis absorption spectroscopy on a UV1900 spectrophotometer (Shanghai Jinghua Tech., China). A Spectrum 100 infrared spectrometer equipped with an ATR accessory (PerkinElmer Inc., USA) was used to obtain the Fourier transform infrared (FTIR) vibrational spectra of samples. A JEOL 2100 (Japan) high-resolution transmission electron microscope (HRTEM) and a Zeiss Ultra plus scanning electron microscope (Germany) were used for the morphological characterization of the AgNPs. The dimension and the mean diameter of the AgNPs were obtained with the aid of ImageJ 1.42 and OriginPro 8 software. An Optima 5300 DV ICP-OES (PerkinElmer Inc., USA) was used to determine the concentration of Ag *via* triplicate analysis of the digested samples. The thermogravimetric analysis (TGA) of the AgNPs was performed on a STA 6000 (PerkinElmer Inc., USA) in the temperature range 25–800 °C. The powder X-ray diffraction (XRD) pattern of the AgNPs was acquired on a Bruker AXS 8 Advance (Germany) over the angular range 2θ = 15–80° at room temperature. The AgNP crystallite size (D_{hkl}) was calculated using Scherrer's formula (eqn (1)), where λ is the X-ray wavelength (0.154 nm), β is the full width at half maximum, determined with the aid of Gaussian fit of the peak (111) using the highest intensity and θ is the corresponding Bragg angle associated with the peak.

$$D_{hkl} = 0.94\lambda/\beta \cos\theta \quad (1)$$

2.5. Catalytic degradation study

The catalytic activity of the biosynthesized AgNPs was evaluated by monitoring the degradation of MB dye using $NaBH_4$. 2 mL of MB dye (10^{-4} M) was added to 1 mL of freshly prepared $NaBH_4$ solution (10^{-2} M) and 0.5 mL of the AgNPs (equivalent to *ca.* 71 nmol of Ag) in a quartz cuvette. The reaction was monitored at regular time intervals on a UV1900 spectrophotometer (Shanghai Jinghua Tech., China). The effect of pH, temperature and higher volume of MB was determined and the pseudo-first-order kinetics was used to establish the rate of reaction and the apparent rate constant was obtained from eqn (2) where A_t, A_0, K_{app} and t are the absorbance at time t, initial absorbance, apparent rate constant, and time taken for the degradation of MB dye in the presence of $NaBH_4$ and the catalyst.

$$\ln(A_t/A_0) = K_{app}t \quad (2)$$

2.6. Antimicrobial activity study

The antimicrobial activities of the PPLE and the biosynthesized AgNPs were investigated against clinical pathogens (*Staphylococcus aureus*, *Salmonella*, *Klebsiella pneumoniae*, *Escherichia coli* and *Pseudomonas aeruginosa*) maintained in nutrient agar at 4 °C in a refrigerator. The inoculum preparation was conducted by transferring the colonies of the organisms into test tubes containing 3 mL of sterile normal saline. These were standardized to 0.5 McFarland turbidity. The as-prepared PPLE (7.1 ± 0.4 g L; dry weight) and the AgNP (15.3 mg L^{-1}) aqueous solutions were taken as 100% and corresponding lower concentrations (12.5%, 25% and 50%) were prepared by serial dilution. In addition, we included the effect of the PPLE : $AgNO_3$ volume and the time of synthesis used in the preparation of the AgNPs on the antimicrobial activities. The PPLE and the biosynthesized AgNPs were screened against the bacteria using the agar well diffusion method. A sterilized cotton swab was dipped into the inoculum and seeded all over the Muller Hinton agar plate by rotating through an angle of 60°. After each swabbing, the swab was passed around the edges of the agar surface and left to dry for a few minutes at room temperature with the lid closed. A sterilized cork borer (6 mm) was used to make four wells in the inoculated plates. Different concentrations of the PPLE and the AgNPs were dispensed in the respective wells using sterilized pipettes. The plates were left for 30 min with the lid closed. Ciprofloxacin (5 μg) was used as a positive control. The incubation was at 37 °C for 24 h. This was followed by observation and measurement of the zones of inhibition around the wells. The assay was conducted in duplicate and the zones of inhibition were expressed as the mean diameter of the clear zones in millimeters.

3. Results and discussion

3.1. The PPLE and the biosynthesized AgNPs

The UV-visible absorption spectrum of the PPLE (Fig. 1A) showed a narrow peak centered at 350 nm. This could be attributed to the presence of electron-rich polyphenols with the π-conjugated system. Generally, polyphenols make electrons available for the reduction of the Ag^+ ions to AgNPs.[24,32,33] At high pH, the polyphenols are deprotonated leading to the creation of an electrostatic attraction and transfer of electrons for the reduction of Ag^+ ions to AgNPs. The oxidized polyphenols also provide stability by coordination to the AgNP surface (Scheme 1). The spectrum of the biosynthesized AgNPs was broad with a peak centered at 485 nm which indicated the surface plasmon resonance of the oscillation electrons on the surface of the AgNPs. The optimum pH for the synthesis of the AgNPs was 9. In comparison, there was no significant increase in absorbance at pH 10. However, at pH 3 the spectrum was extensively broad with a reduction in absorbance while at neutral pH the spectrum was similarly broad with an increase in absorbance. The synthesis of the AgNPs was completed in 45 min (Fig. 1B). Increase in the volume of the extract significantly improved the absorbance peak with the optimum absorbance attained at a volume ratio of 20/4 (extract : $AgNO_3$). A higher volume ratio resulted in no significant increase in absorbance (Fig. 1C). The broadness of the spectrum indicates the polydispersity of the NPs. There are related broad spectra observed for AgNPs synthesized *via* plant extracts from pods of PP,[10] and leaves of *Tagetes lemmonii*[24] and *catharanthus roseus*[34] with peaks centered at 407, 453 and 480 nm, respectively. The

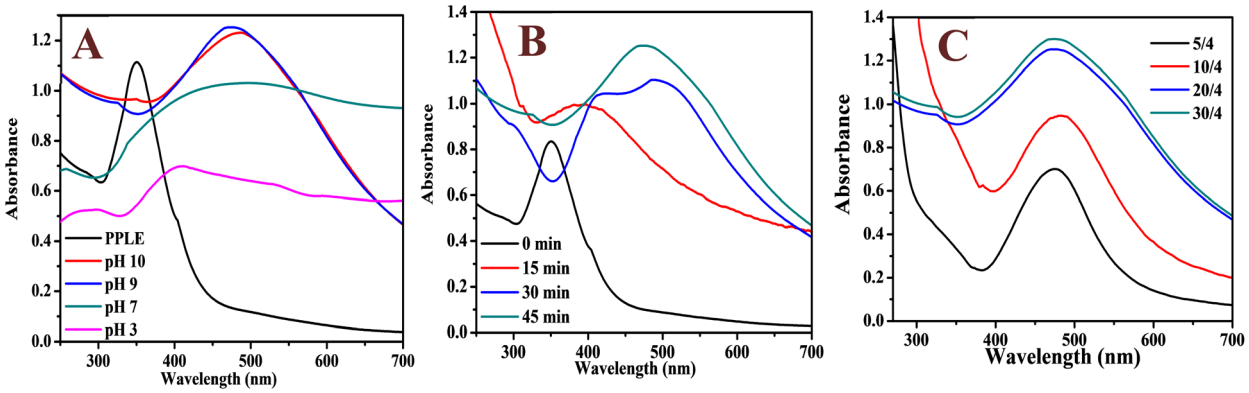

Fig. 1 UV-vis spectra of (A) the PPLE and the AgNPs synthesized at different pH, (B) time and (C) using different volumes of PPLE.

deep brownish coloration of the AgNP solution in comparison to the yellow color of PPLE indicated the presence of the AgNPs. The Ag content of the AgNPs synthesized under optimum conditions is 15.3 ± 3.4 mg L^{-1} as established by triplicate analysis of microwave digested sample on an ICP-OES.

3.2. FTIR study

The functional groups associated with compounds present in the PPLE and the biosynthesized AgNPs were revealed using FTIR analysis, which indicated the presence of –OH/–NH_2, –C–$H_{str.}$, –C═C, –C–OH, –C–O–C and –C–H_{bend} with the corresponding vibrational bands at (ν/cm^{-1}) 3408, 2941, 1618, 1388, 1216, 1100 and 770 respectively (Fig. 2).[10,13,25] These functional groups provided evidence for the presence of phytochemical constituents (flavonoids, terpenoids, polyphenols, steroids, tannins, glycosides, and alkaloids) of the PPLE.[6,13,14] The compounds provided the electrons that induced the reduction of Ag^+ ions and also stabilized the subsequently developed AgNPs. The mechanism involves the coordination of the Ag^+ ions to the compounds *via* the heteroatoms (O and N) and this is accompanied by the transfer of electrons for the reduction of Ag^+ ions. The Ag atoms formed serve as nucleation points for further reduction and the growth of the AgNPs. The presence of the phytochemicals was also confirmed using the FTIR spectrum of the AgNPs, which also revealed similar vibrational bands with a slight shift in wavenumber, an indication of their influence on the stabilized AgNPs (Fig. 2).

3.3. Powder X-ray diffraction study of the AgNPs

The diffractogram obtained from the XRD analysis of the AgNPs (Fig. 3) showed a diffraction pattern associated with Ag metal with peaks at 2θ = 38.1°, 44.3°, and 64.8° corresponding respectively to the (111), (200), and (220) planes of the face centered cubic lattice established for Ag metal according to the

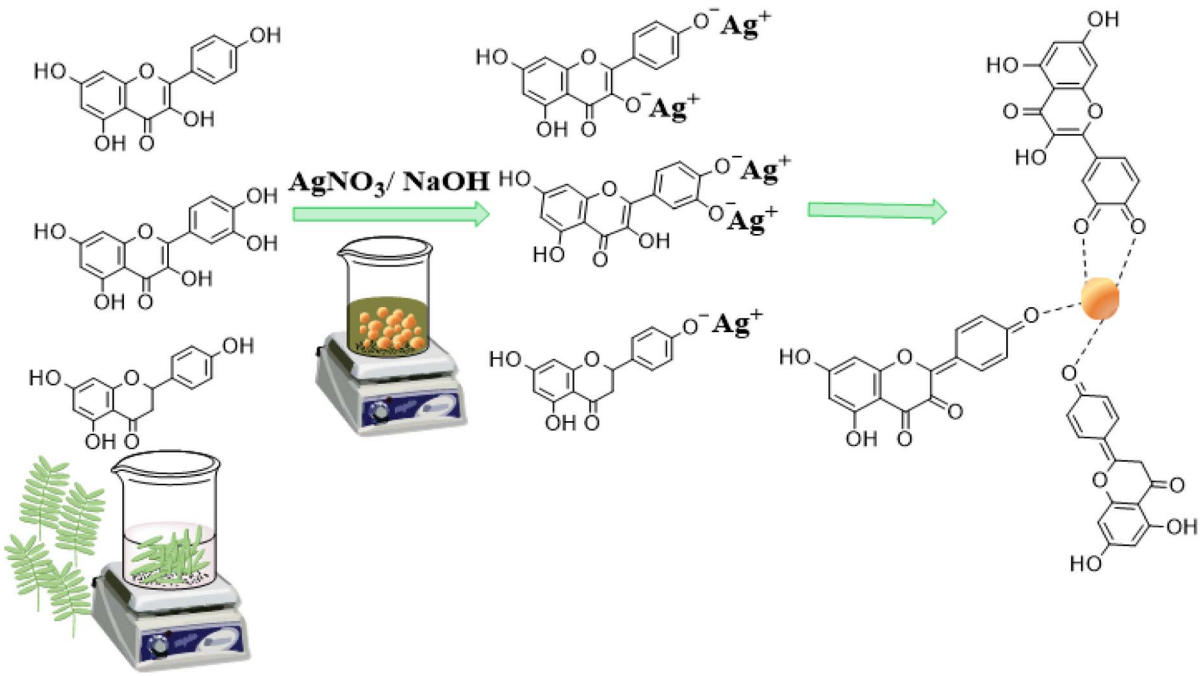

Scheme 1 Illustration of the reaction mechanism for the AgNP synthesis.

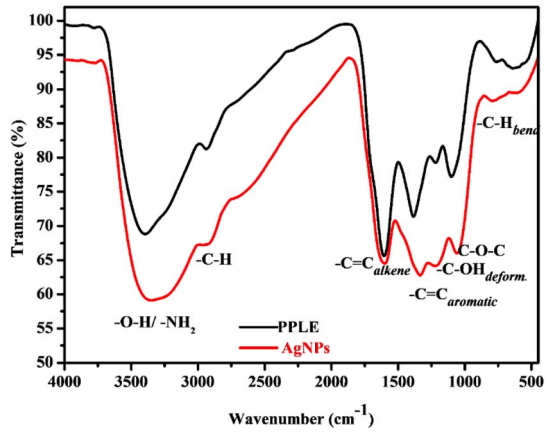

Fig. 2 FTIR spectra of the PPLE and the AgNPs.

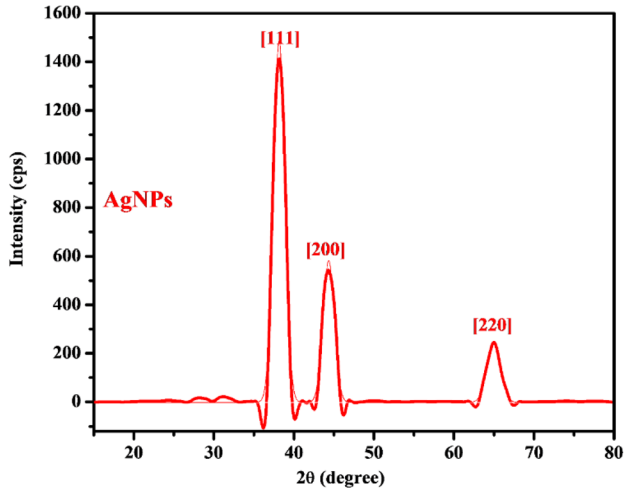

Fig. 3 The XRD pattern of the AgNPs.

Joint Committee on Powder Diffraction Standard record (JCPDS File no. 04-0783). The prominence of the peaks supports the crystalline nature of the AgNPs as observed in the SAED on the HRTEM. The calculated crystallite size (5.7 nm) indicated the size of a single nanocrystal which combined to form the various observed dimensions of the AgNPs as observed in HRTEM micrographs. Similar diffraction patterns have been reported for AgNPs synthesized using extracts of other plants.[10,23,35]

3.4. TGA/DTA study of the AgNPs

The thermogram obtained from the TGA analysis of the AgNPs (Fig. 4) revealed the presence of moisture, volatile organic components and thermally stable material. The thermal degradation occurred in two temperature regions with different percentage mass losses in the ranges 25–200 °C (7%) and 200–750 °C (47%) while a relatively stable composition was observed in the temperature range 750–800 °C. The observed mass losses indicated the release of surface moisture, volatile constituents and major organic compounds present in PPLE, which

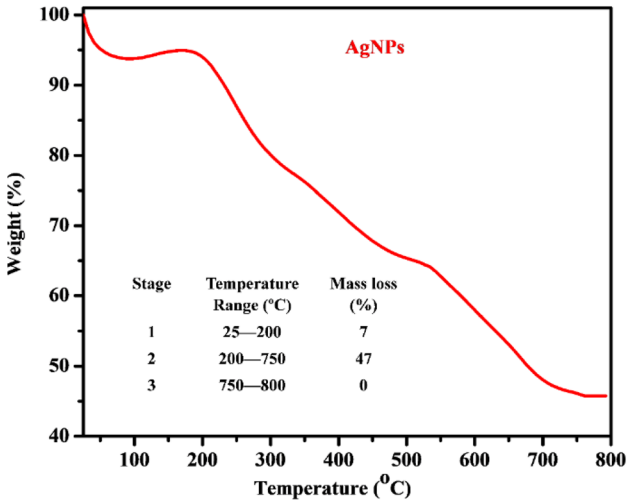

Fig. 4 Thermogram and thermal analysis data (inset) of the AgNPs.

stabilized the AgNPs. This observation correlates with the surface coating on the AgNPs revealed by the SEM micrograph and the functional groups indicated by the FTIR spectra of the PPLE and the AgNPs. The different chemical decomposition was revealed by the fluctuation in the slope. The residual mass (46%) at 800 °C indicated the thermally stable Ag metal left after the loss of the organic components.

3.5. Morphological study of the AgNPs

Dispersed spherically shaped AgNPs were revealed by the representative HRTEM micrograph (Fig. 5A) of the AgNPs. However, the effect of strong interfacial interaction between the NPs was observed to result in formation of quasi-spherical and elliptical morphological structures as the small NPs combined together. Despite the interaction, the individual NPs were well dispersed without excessive aggregation, which indicated the influence of the phytochemicals in the stabilization of the AgNPs in the colloidal sample. The selected area electron diffraction (SAED) patterns (Fig. 5A; inset) showed distinct rings suggesting the crystalline nature of the AgNPs.[36,37] The observed lattice fringes with an average inter-particle spacing of 0.253 ± 0.027 nm correspond to the (111) plane of face-centered cubic Ag metal.[36,38] The size distribution graph (Fig. 5B) showed a narrow range (2–50 nm) for the particle population with a mean of 19 nm. At pH 3 large AgNPs were observed, while a mixture of large and small AgNPs was observed at neutral pH. However, at pH 9 the AgNPs were well shaped with a narrow size range (Fig. 5A: inset). Unlike the colloidal sample used for the HRTEM, the dry sample used for the acquisition of the SEM micrograph (Fig. 5C) constituted aggregates of the AgNPs with a rough and porous surface. This suggested the coating of the NPs by the phytochemicals, which stabilized the NPs. The aggregates resulted from the drying effect. The individual NP can be easily recovered after dispersion in solvent and sonication. Similar size and morphology have been reported by Nima *et al.* for AgNPs synthesized using broths of leaves (20 nm) and pods (15 nm) of PP.[39]

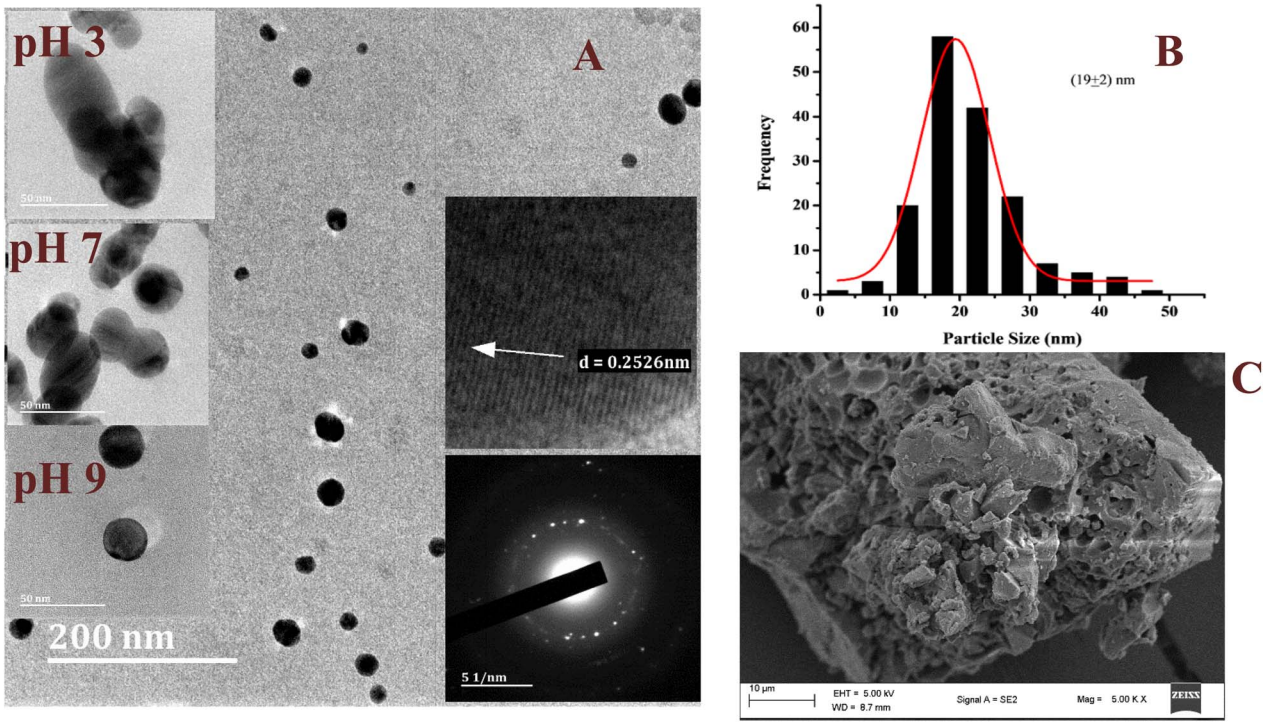

Fig. 5 The representative HRTEM micrograph of the AgNPs synthesized under optimum conditions, inset; HRTEM micrographs at different pH, selected area electron diffraction and the lattice fringes (A), the particle size distribution (B), and the SEM micrograph of the AgNPs (C).

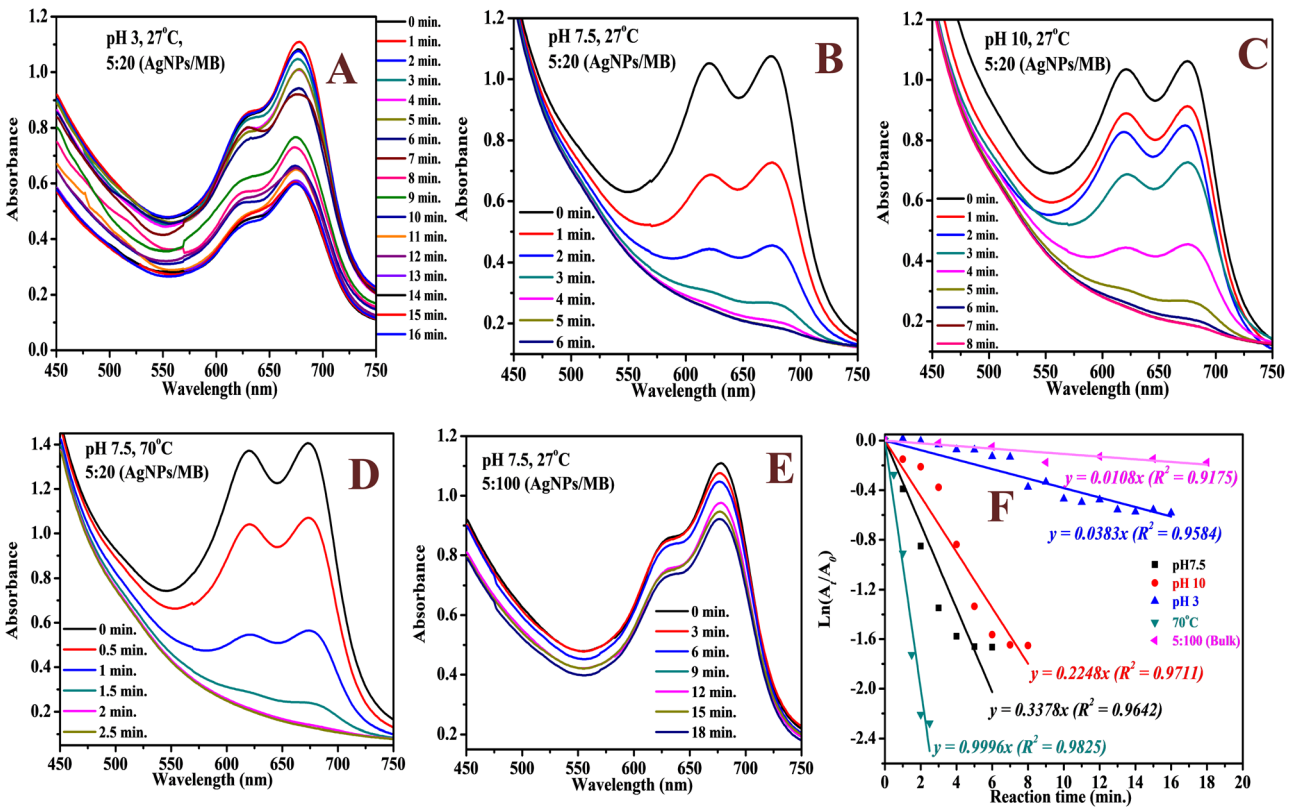

Fig. 6 The UV-vis spectra of the catalytic degradation of MB dye using the AgNPs at pH 3 (A), pH 7.5 (B), pH 10 (C), 70 °C (D), high volume of MB dye (E) and the corresponding kinetic plot (F).

3.6. Catalytic degradation of MB dye using the AgNPs

The catalytic activity of the biosynthesized AgNPs was evaluated *via* the chemical degradation of MB dye monitored with a UV-vis spectrophotometer. The rate of degradation was very slow without a catalyst. The presence of the AgNPs as a catalyst increased the rate of the reaction rapidly and reduced the reaction time considerably. The reduction in the absorbance of the most intense peak at 665 nm, a characteristic of MB dye, was monitored with time (Fig. 6). The degradation of MB dye in the presence of the AgNPs reached a maximum (82%) within 6 min at optimum pH (7.5) as revealed by the reduction in absorbance (Fig. 6) with a corresponding high pseudo-first order rate constant (0.3378 min^{-1}). After 82% degradation, the catalyst surface becomes saturated with the product which hinders further degradation. The rate constant drastically reduced to 0.0383 min^{-1} in acidic medium (pH 3) and only 44% degradation was observed after 16 min. This was expected as the presence of excess protons could limit the interaction of the cationic dye at the AgNP surface. At pH 10, 81% degradation was achieved in 8 min. The high pH will introduce more negative charge (OH^-) on the catalyst surface and limit the surface interaction of the reducing agent (BH_4^-) at the surface of the AgNPs. Hence, the neutral pH was most suitable. The rate of degradation was rapid when the temperature was raised to 70 °C and 90% degradation was recorded in 2.5 min. This shows greater collision with higher energy leading to rapid degradation. The degradation suffered a setback when the volume proportion of MB was increased by 5 fold; 16% degradation was achieved after 18 min. This shows that the surface of the AgNPs has been saturated with the dye molecules and the reducing agent may not have good contact with the surface. A color change from blue to colorless was observed at pH 7.5 and 10 as well as at high temperatures, which indicated the formation of leucoMB dye which is less harmful to the environment. Degradation was facilitated by the transition of electrons from $NaBH_4$ to MB dye through the AgNPs, which provided an electron-rich surface for interaction between the reactants. It is important to note that the phytochemicals stabilizing the AgNPs can aid in the attraction of the dye molecules to the surface of the AgNPs *via* hydrophobic interaction and van der Waals forces. The AgNPs demonstrated comparative catalytic performance among other AgNPs synthesized using different plant extracts as presented in Table 1. The catalyst maintained a relatively stable catalytic performance (Fig. 7A) and there was no observable change in morphology after 5 cycles as revealed by the HRTEM micrograph of the recovered NPs (Fig. 7B).

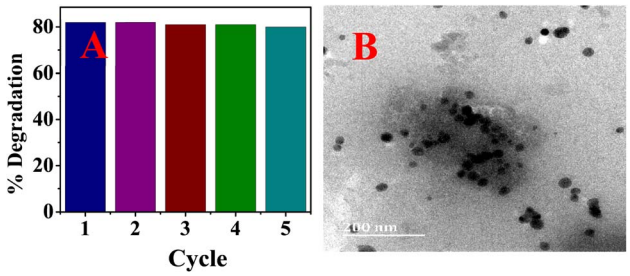

Fig. 7 Catalytic performance for 5 cycles (A) and the HRTEM micrograph (B) of the recovered AgNPs after the 5th cycle.

3.7. Antimicrobial activities of the PPLE and the AgNPs

The results of the antimicrobial activities of the PPLE and the AgNPs against the clinical pathogens are shown in Table 2.

The inhibition of the bacteria by the PPLE and the AgNPs was observed to increase with respect to concentration. The bacteria were more susceptible to the AgNPs at the highest concentration than the PPLE. The PPLE and the AgNPs showed the greatest inhibition against *P. aeruginosa*. However, *S. aureus* and *K. pneumoniae* were most resistant to the PPLE and the AgNPs, respectively. The greater susceptibility of Gram-negative bacteria (*Salmonella*, *K. pneumoniae*, *E. coli* and *P. aeruginosa*) to the PPLE indicated the capacity of the phytoconstituents to disrupt the intracellular activity after easily penetrating the thin peptidoglycan layer of the cell wall unlike the thick peptidoglycan layer of the Gram-positive (*S. aureus*) cell wall.[33,45] However, the AgNPs might have adopted another mode of inhibition of the pathogens, which were indiscriminately inhibited irrespective of the structural components of their cell wall. The presence of phytochemicals serving as a stabilizing agent as revealed by FTIR spectra and SEM micrograph can aid the AgNPs to easily bind, interact and penetrate the cell *via* hydrophobic interaction and van der Waals forces. This can cause the disruption of cellular activity through the release of Ag^+ ions leading to the formation of reactive oxygen species,

Table 1 Comparison of AgNP size, catalytic degradation time and rate constant of MB dye in the presence of AgNPs synthesized with different plant extracts

Plant/part	AgNP size (nm)	Time (min)	Rate const. (min^{-1})	%Degrad.	Ref.
Peltophorum pterocarpum/leaf	2–50	6	0.3378	82	This study
Convolvulus arvensis/leaf	28	20	0.1080	—	40
Picrasma quassioides/bark	17–67	30	0.0660	—	41
Achillea millefolium	20	13	—	—	42
Gmelina arborea/fruit	8–32	10	—	100	43
Trigonella foenum-graecum/seed	10–30	8	1.0200	—	44
Eulophia herbacea/tuber	12	30	—	—	30
Diplazium esculentum/leaf	6–47	90	0.1051	91	32

Table 2 The antibacterial activity of PPLE and AgNPs against selected pathogens including the effect of the volume of PPLE and time used for the synthesis of the AgNPs

	PPLE				PPLE/AgNPs				Ciprofloxacin
	12.50%	25.00%	50.00%	100.00%	12.50%	25.00%	50.00%	100.00%	5 μg
Test organism	Zones of inhibition in millimetre (mm)								
S. aureus	0 ± 0	8 ± 1	10 ± 3	12 ± 1	10 ± 1	12 ± 0	13 ± 1	17 ± 1	21 ± 0
E. coli	8 ± 1	11 ± 0	11 ± 1	12 ± 3	10 ± 1	13 ± 1	15 ± 2	16 ± 1	26 ± 0
Salmonella spp.	8 ± 0	10 ± 1	11 ± 3	14 ± 1	12 ± 3	15 ± 1	15 ± 1	16 ± 1	24 ± 0
K. pneumoniae	9 ± 1	11 ± 1	12 ± 1	13 ± 0	11 ± 0	12 ± 3	14 ± 3	15 ± 3	25 ± 0
P. aeruginosa	10 ± 1	12 ± 3	15 ± 1	15 ± 3	12 ± 3	16 ± 1	17 ± 3	20 ± 1	26 ± 0

	PPLE/AgNPs ratio				PPLE/AgNP reaction time (min.)			
	5/4	10/4	20/4	30/4	0	15	30	45
Test organism	Zones of inhibition in millimetre (mm)							
S. aureus	13 ± 2	13 ± 1	17 ± 1	16 ± 0	3 ± 1	7 ± 2	11 ± 0	17 ± 1
E. coli	12 ± 1	12 ± 0	16 ± 1	17 ± 2	8 ± 0	11 ± 1	14 ± 1	16 ± 1
K. pneumoniae	10 ± 0	12 ± 2	15 ± 3	15 ± 0	0 ± 0	3 ± 1	5 ± 0	15 ± 3
P. aeruginosa	14 ± 2	12 ± 1	20 ± 1	20 ± 3	0 ± 0	0 ± 0	7 ± 1	20 ± 1

peroxidation, denaturation of essential proteins of the bacteria, inhibition of the replication of the DNA and damage of organelles as well as leakage of cytoplasm resulting from cell membrane perforation (Scheme 2). This will result in lethal conditions that can ultimately lead to cell death.[46,47] Further investigation revealed that the volume ratio of the extract to metal precursor and the duration used for the synthesis of the AgNPs also significantly influence the antibacterial activities. An increment in inhibition was observed with respect to increasing volume ratio and this suggested presence of more reactive AgNPs against the bacteria as the higher volume ratio provided more reducing and stabilizing agents. However,

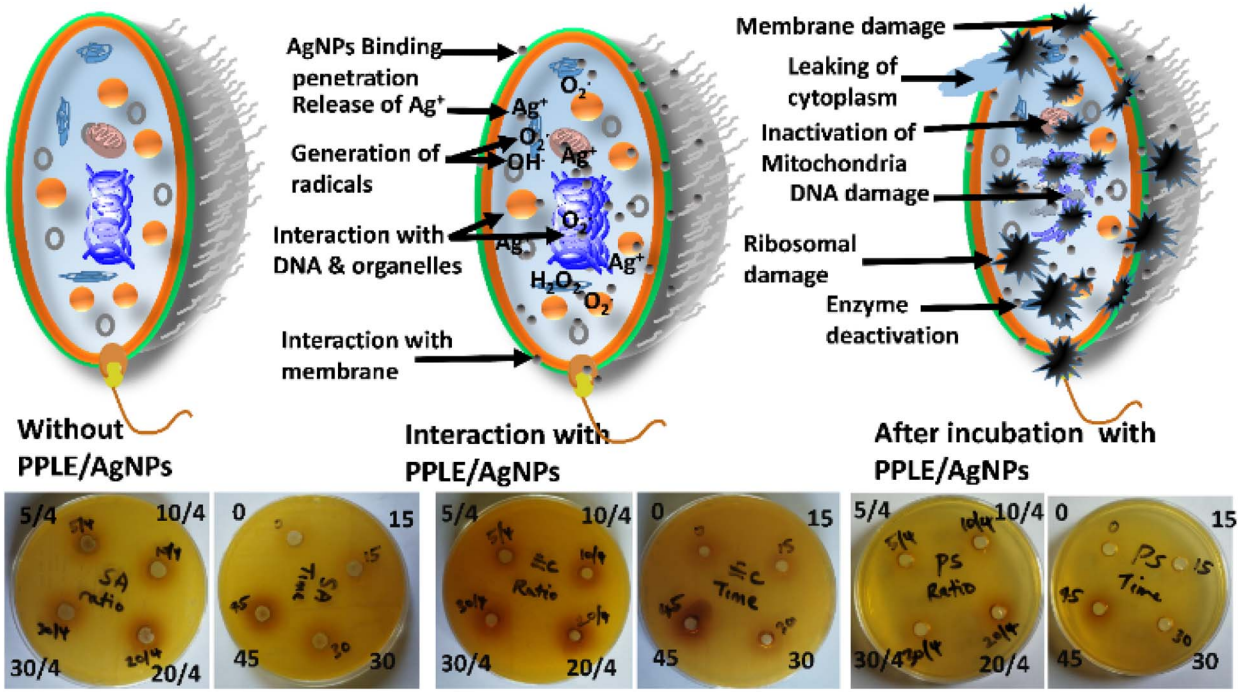

Scheme 2 Illustration of the antibacterial mode of action of the AgNPs against selected pathogens including the representative plates showing the zones of inhibition in *S. aureus*, *E. coli* and *P. aeruginosa* with respect to volume (5/4, 10/4, 20/4 and 30/4) of PPLE and time (0, 15, 30 and 45 min) used to synthesize the AgNPs.

a further increase in the volume ratio above the optimum (20/4) shows no significant increment. The AgNPs obtained at the optimum reaction time (45 min) show the greatest effect. This can be attributed to the presence of more AgNPs. Since AgNPs have been found effective against multi-drug resistant (MDR) bacteria, the synthesized PPLE/AgNPs can help to combat the drug-resistant mechanism associated with MDR bacteria as they exhibit an indiscriminate mode of action and interact with multiple targets *via* the generation of reactive oxygen species leading to inactivation of several cellular activities.[48–50] Our findings align with the report on the antimicrobial activities of methanolic extract of PP flowers which indicated that the Gram-negative bacteria were more susceptible, with *P. aeruginosa* showing the least resistance.[2] Another report on AgNPs biosynthesized with pod extract of PP showed dose-dependent inhibition against *E. coli* as also observed in this study.[10] *P. aeruginosa* was also reported to be most susceptible to AgNPs synthesized using *Mentha aquatica* leaf extract.[51]

4. Conclusions

AgNPs were biosynthesized using PPLE as a source of phytochemicals and served the dual function of both reducing- and stabilizing agents. The UV-visible and the FTIR spectra showed absorbance that indicated the presence of chromophoric compounds and functional groups associated with polyphenolic compounds present in the PPLE. The UV-vis spectrum of the biosynthesized AgNPs showed broad peak absorbance at 485 nm characteristic of AgNPs resulting from plasmonic resonance of the electrons at the surface of the NPs. The FTIR spectrum of the AgNPs revealed functional groups of the phytochemicals that provide stability for the AgNPs. The AgNPs were observed to be in the range 2–50 nm as revealed by the HRTEM with many adopting distorted spherical morphology. The presence of phytochemicals on the AgNPs was further established by the observed surface roughness of the NPs resulting from the coating with phytochemicals and the non-uniform thermal degradation as revealed by the SEM micrograph and the TGA thermogram respectively. The AgNPs exhibited good catalytic activity for the degradation of MB dye within 5 min and also demonstrated antibacterial activities against selected pathogens. This study thus provides evidence in support of the biosynthesized AgNPs using the PPLE as a potential catalyst and antimicrobial agent suitable for the degradation of dye and they can also be incorporated into formulations of products containing AgNPs such as disinfectants.

Author contributions

S. A. Ogundare: writing-original draft, conceptualization, methodology. T. O. Adesetan: writing-original draft, methodology. G. Muungani: formal analysis, investigation. V. Moodley: formal analysis, investigation. J. F. Amaku: data curation and investigation. O. C. Atewolara-Odule: project administration, formal analysis. S. T. Yussuf: project administration, visualization. N. O. Sanyaolu: visualization, data curation. A. A. Ibikunle: investigation, supervision. M.-S. Balogun: supervision, investigation. W. E. van Zyl: resources, supervision, writing – review & editing.

Conflicts of interest

There are no conflicts to declare.

Acknowledgements

W. E. V. Z. gratefully acknowledges support in part by the National Research Foundation of South Africa (Grant Number: 132014), and the Eskom TESP program. S. A. O. and T. O. A. acknowledge the support granted by Ogunlade Jesuloluwa, Omotayo Oreoluwa, Ayoola Esther and Adegbesan Opeyemi.

References

1 P. Muthukumaran, N. Saraswathy, V. Aswitha, R. Balan, V. B. Gokhul, P. Indumathi and S. Yuvapriya, *Pharmacogn. J.*, 2016, **8**, 140–143.
2 S. Sukumaran, S. Kiruba, M. Mahesh, S. Nisha, P. Z. Miller, C. Ben and S. Jeeva, *Asian Pac. J. Trop. Med.*, 2011, **4**, 735–738.
3 M. Babu, A. Anand, F. Hakkim and Q. Haq, *Int. J. Adv. Res.*, 2016, **4**, 801–807.
4 R. Jagessar, A. Mohamed and G. Gomes, *Nat. Sci.*, 2007, **5**, 81–93.
5 R. Jha, P. T. Ramani, D. Patel, S. Desai and D. Meshram, *J. Med. Plants Stud.*, 2016, **4**, 18–22.
6 O. E. Taiwo, M. O. Efere, M. A. Joseph and A. A. Saburi, *J. Pharmacogn. Phytother.*, 2013, **5**, 77–82.
7 O. Enechi, A. Mbahotu and U. R. Ikechukwu, *Am.-Eurasian J. Agric. Environ. Sci.*, 2016, **16**(4), 836–841.
8 M. Karunai Raj, C. Balachandran, V. Duraipandiyan, P. Agastian, S. Ignacimuthu and A. Vijayakumar, *Med. Chem. Res.*, 2013, **22**, 3823–3830.
9 S.-R. Kim, D. Cuong To, P. H. Nguyen, Y. N. Nguyen, B.-J. Cho and M. H. Tran, *Molecules*, 2020, **25**, 4800.
10 S. Raja, V. Ramesh and V. Thivaharan, *J. Ind. Eng. Chem.*, 2015, **29**, 257–264.
11 T. Manaharan, L. L. Teng, D. Appleton, C. H. Ming, T. Masilamani and U. D. Palanisamy, *Food Chem.*, 2011, **129**, 1355–1361.
12 M. Hait, P. T. Sisodiya and A. Patel, *J. Pharmacogn. Phytochem.*, 2017, **6**, 270–272.
13 P. Sanjay, K. Deepa, J. Madhavan and S. Senthil, *Mater. Lett.*, 2018, **219**, 158–162.
14 P. Sanjay, K. Deepa, J. Madhavan and S. Senthil, *Opt. Mater.*, 2018, **83**, 192–199.
15 P. Sanjay, K. Deepa, M. V. A. Raj, J. Madhavan and S. Senthil, *Mater. Today: Proc.*, 2019, **8**, 123–129.
16 I. C. Maurya, A. K. Gupta, P. Srivastava and L. Bahadur, *Opt. Mater.*, 2016, **60**, 270–276.
17 S. K. Jash, R. K. Singh, S. Majhi, A. Sarkar and D. Gorai, *Int. J. Pharm. Sci. Res.*, 2013, **5**, 26–36.
18 J. Polasek, E. F. Queiroz, L. Marcourt, A. K. Meligova, M. Halabalaki, A.-L. Skaltsounis, M. N. Alexis, B. Prajogo,

J.-L. Wolfender and K. Hostettmann, *Planta Med.*, 2013, **79**, 480–486.
19 Y.-C. Li, P.-C. Kuo, M.-L. Yang, T.-Y. Chen, T.-L. Hwang, C.-C. Chiang, T. D. Thang, N. N. Tuan and J. T. Tzen, *Molecules*, 2019, **24**, 240.
20 T. Masilamani, T. Subramaniam, N. Nordin and R. Rosli, *Clin. Phytosci.*, 2017, **3**, 1–13.
21 A. Dash, M. T. Ahmed and R. Selvaraj, *J. Mol. Struct.*, 2019, **1178**, 268–273.
22 S. Pai, H. Sridevi, T. Varadavenkatesan, R. Vinayagam and R. Selvaraj, *Optik*, 2019, **185**, 248–255.
23 S. Jain and M. S. Mehata, *Sci. Rep.*, 2017, **7**, 1–13.
24 K. Chandhirasekar, A. Thendralmanikandan, P. Thangavelu, B.-S. Nguyen, T.-A. Nguyen, K. Sivashanmugan, A. Nareshkumar and V.-H. Nguyen, *Mater. Lett.*, 2021, **287**, 129265.
25 R. Vinayagam, S. Pai, G. Murugesan, T. Varadavenkatesan and R. Selvaraj, *Appl. Nanosci.*, 2021, 1–11.
26 V. C. Karade, R. B. Patil, S. B. Parit, J. H. Kim, A. D. Chougale and V. V. Dawkar, *ACS Sustainable Chem. Eng.*, 2021, **9**, 12476–12507.
27 T. Benn, B. Cavanagh, K. Hristovski, J. D. Posner and P. Westerhoff, *J. Environ. Qual.*, 2010, **39**, 1875–1882.
28 R. Kessler, *Environ. Health Perspect.*, 2011, **119**, A120–A125.
29 C. Cascio, O. Geiss, F. Franchini, I. Ojea-Jimenez, F. Rossi, D. Gilliland and L. Calzolai, *J. Anal. At. Spectrom.*, 2015, **30**, 1255–1265.
30 J. S. Pawar and R. H. Patil, *SN Appl. Sci.*, 2020, **2**, 1–12.
31 S. Anchan, S. Pai, H. Sridevi, T. Varadavenkatesan, R. Vinayagam and R. Selvaraj, *Biocatal. Agric. Biotechnol.*, 2019, **20**, 101251.
32 A. A. Hadi, J. Y. Ng, M. Shamsuddin, J. Matmin and N. A. N. N. Malek, *Chem. Pap.*, 2022, **76**, 65–77.
33 S. Donga and S. Chanda, *Artif. Cells, Nanomed., Biotechnol.*, 2021, **49**, 292–302.
34 S. Anjum and K. Riazunnisa, *Res. J. Chem. Environ.*, 2021, **25**, 5.
35 E. E. Elemike, D. C. Onwudiwe, A. C. Ekennia, R. C. Ehiri and N. J. Nnaji, *Mater. Sci. Eng., C*, 2017, **75**, 980–989.
36 O. S. Oluwafemi, T. Mochochoko, A. J. Leo, S. Mohan, D. N. Jumbam and S. P. Songca, *Mater. Lett.*, 2016, **185**, 576–579.
37 T. N. J. I. Edison, M. G. Sethuraman and Y. R. Lee, *Res. Chem. Intermed.*, 2016, **42**, 713–724.
38 S. A. Ogundare and W. E. van Zyl, *Surf. Interfaces*, 2018, **13**, 1–10.
39 P. Nima, A. Astalakshmi and V. Ganesan, *The Journal of Bioprocess Technology, Photon*, 2013, **98**, 308–317.
40 S. Hamedi, S. A. Shojaosadati and A. Mohammadi, *J. Photochem. Photobiol., B*, 2017, **167**, 36–44.
41 T. Sreekanth, M.-J. Jung and I.-Y. Eom, *Appl. Surf. Sci.*, 2016, **361**, 102–106.
42 B. Khodadadi, M. Bordbar and M. Nasrollahzadeh, *J. Colloid Interface Sci.*, 2017, **493**, 85–93.
43 J. Saha, A. Begum, A. Mukherjee and S. Kumar, *Sustainable Environ. Res.*, 2017, **27**, 245–250.
44 V. Vidhu and D. Philip, *Micron*, 2014, **56**, 54–62.
45 D. Bharathi, M. Diviya Josebin, S. Vasantharaj and V. Bhuvaneshwari, *J. Nanostruct. Chem.*, 2018, **8**, 83–92.
46 J. Cheng, X. Lin, X. Wu, Q. Liu, S. Wan and Y. Zhang, *Int. J. Biol. Macromol.*, 2021, **188**, 678–688.
47 T. Sowmyya, *J. Environ. Chem. Eng.*, 2018, **6**, 3590–3601.
48 V. C. Karade, R. B. Patil, S. B. Parit, J. H. Kim, A. D. Chougale and V. V. Dawkar, *ACS Sustainable Chem. Eng.*, 2021, **9**, 12476–12507.
49 S. Hamedi, S. A. Shojaosadati and A. Mohammadi, *J. Photochem. Photobiol., B*, 2017, **167**, 36–44.
50 M. A. Hussain, A. Shah, I. Jantan, M. N. Tahir, M. R. Shah, R. Ahmed and S. N. A. Bukhari, *J. Nanobiotechnol.*, 2014, **12**, 53.
51 A. Nouri, M. T. Yaraki, A. Lajevardi, Z. Rezaei, M. Ghorbanpour and M. Tanzifi, *Colloid Interface Sci. Commun.*, 2020, **35**, 100252.